electronics

MDPI

Article

Development of a Wearable System for the Detection of Ingestible Medication Based on Electromagnetic Waves

Junya Hoshino, Jaakko Hyry, Takumi Kobayashi and Daisuke Anzai *

Graduate School of Engineering, Nagoya Institute of Technology, Nagoya 466-8555, Japan; hyry.jaakko@nitech.ac.jp (Jaakko Hyry); kobayashi@nitech.ac.jp (T.K.)
* Correspondence: anzai@nitech.ac.jp; Tel.: +81-52-735-5389

Abstract: Managing medication status solves related complications and prevents increases in medical costs due to the improper management of prescriptions. An ingestible sensor can be used to confirm a patient's real-time medical status by measuring the electromagnetic waves transmitted from an ingested medication from outside of the human body. However, concerns about costs of delivery arise, as it would be necessary to attach a sensor to each ingested medication. In this study, we focused on using an electromagnetic (EM) imaging method which can estimate the internal structure of various objects using a scattered electric field. With this method we can detect medication as it does not require the installation of a sensor. At first we performed an electromagnetic field simulation and based on the results we experimentally measured the external electric field, which changes with the medicine. Then, we evaluated the accuracy of the detection method by calculating the difference between the detection rate with the proposed detection method against a more conventional method. The results indicate the possibility of achieving a more than 20% higher accuracy than the conventional detection method with our proposed method using electromagnetic waves.

Keywords: EM imaging; human body communication; ingestible digital medication

check for updates

Citation: Hoshino, J.; Hyry, J.; Kobayashi, T.; Anzai, D. Development of a Wearable System for the Detection of Ingestible Medication Based on Electromagnetic Waves. *Electronics* **2024**, *13*, 543. https://doi.org/10.3390/electronics13030543

Academic Editors: Reza K. Amineh and Hristos T. Anastassiu

Received: 7 December 2023
Revised: 21 January 2024
Accepted: 26 January 2024
Published: 29 January 2024

Copyright: © 2024 by the authors. Licensee MDPI, Basel, Switzerland. This article is an open access article distributed under the terms and conditions of the Creative Commons Attribution (CC BY) license (https://creativecommons.org/licenses/by/4.0/).

1. Introduction

In recent years, the shortage of medical staff has become a problem in Japan due to the declining birthrate and the rising aging population, and there are concerns that the quality of medical care will decline even further in the coming years. Furthermore, it is important to reduce the burden on the staff by improving treatment efficiency and to increase patient adherence. Body area networks (BANs) have attracted a great deal of attention as a technology to realize these goals, and the development of BANs has greatly advanced medical care [1,2] in various ways already.

A BAN is a wireless communication technology used on the human body and is generally divided into two types: on-body BAN (e.g., wearable sensors) and in-body BAN (e.g., implants or pills), and was standardized as IEEE 802.15.6 [3] in February 2012. On-body BAN is a technology for constructing a network between wireless terminals placed on the surface of the human body, and is applied to daily monitoring of biological information such as blood pressure [2].

In-body BAN is a technology to build a network inside and outside of the human body by using devices implanted in the body or taken via an ingested pill. With these solutions, the development of implanted or ingested medical devices has been actively carried out. Examples of these are the wireless capsule endoscopy (WCE) and the detection of medicines [4].

Before WCE, we have frequently used wired endoscopy, which has some demerits as the patients experience pain when they are swallowing the endoscopy tube. Furthermore, there is a limit on which organs can be diagnosed by using this method. In contrast, if we use WCE the result is less stress and pain for the patients since they only need to swallow

a small-sized capsule. This also makes it possible to diagnose all digestive organs. Thus, WCE has garnered a lot of attention as an advanced medical solution.

Regarding the detection of medicine, a currently used method is to attach an ingestible sensor to the medicine being studied. When the medicine is swallowed, the next step is to wait for it to be dissolved. This is due to the sensor needing to react with gastric acids to be able to create electricity and start to transmit electromagnetic waves at, e.g., the 2.4 GHz band. Afterwards, a patient's medical status can be confirmed by measuring the transmitted waves from outside of the body. As an example of an existing solution, digital medicine has been proposed [5], where an ultra-small wireless transmitter is embedded into a pill and medication adherence is performed based on the detection of wireless signals. The transmit signal power should be strictly limited due to the size limitation of pills, so we need to consider the detection coverage. On the other hand, our proposed system considers a transmitter outside the human body, so the transmit power limitation can be loosened. Furthermore, only electromagnetic material is required in our proposed system. Hence, a wireless communication circuit would no longer be needed inside the pills. With the increase in the number of prescriptions issued, there have been problems such as adverse complications and an increase in medical expenses due to the improper administration of prescriptions. This is especially common for elderly patients, and will likely become an even greater problem in the future as the birthrate declines. However, attaching an ingestible sensor to medication also creates cost concerns as a sensor is needed for each pill. Additionally, the medicine cannot be detected until it dissolves in the stomach and reacts with the acids. Furthermore, these implant devices might remain inside a patient's body due to unexpected malfunctions and require roentgen as well as possible excision procedures. These impose an extra burden for both patients and healthcare staff. With the demerits of the various methods described above, alternative and less intrusive methods are currently being proposed, using technologies that can be applied for the detection of objects inside the human body. For example, for the detection of objects, received signal strength indicator (RSSI) and time of arrival (TOA) methods have been researched. They both utilize a signal transmitted by the object itself [6–9].

RSSI is a position estimation technology, which utilizes the fact that the signal emitted from the transmitting implant device is attenuated depending on the distance. TOA on the other hand is a position estimation technology, where the signal transmitted from the implant device arrives at different times depending on the distance to each receiver. However, when we use these methods, since we need a wireless channel model inside the human body, a large-scale measurement phase such as computed tomography (CT) or magnetic resonance imaging (MRI) is needed in order to obtain the internal structure of the human body in advance. In addition, when compared with X-ray systems, the proposed method just detects electromagnetic materials based on EM imaging. Hence, the proposed method has the advantages of having a simpler system configuration and a lower human impact than X-ray systems. One of our main goals is to confirm patients' medication adherence, as intakes of medication that are too large or irregular are a problem nowadays. To achieve this, we need to track the intake, and so we experiment on a non-intrusive method with the electromagnetic materials incorporated into, e.g., a pill. If we can confirm the patient has taken their medication, we can improve the treatment outcome.

Therefore, this study focuses on using EM imaging as the medication detection method, as it does not require the installation of a separate sensor. This is achieved with EM imaging using a technique that estimates the internal structure of various objects using a scattered electric field [10]. Furthermore, since the electrical and magnetic constants of the detection target and human tissue are significantly different, it is possible to use detection which does not require prior measurement of the channel model in the human body. An example of this is the position estimation of the capsule endoscope, which can be achieved by measuring and processing the scattered electric field generated when the human body is irradiated with electromagnetic waves. As a typical position estimation method for implant devices by EM imaging there is the greedy method, in which each scattered electric field is obtained

in advance, where an implant device is placed in each cell of the human body model. However, there is a problem as this method requires the use of several measurement points, so the amount of calculations often becomes large and the experimental environment becomes complicated.

Therefore, this study aims to determine the presence or absence of medicine by using an EM imaging method with only a small number of measurement points. To achieve this, we can mix electromagnetic materials with the medicine, and a large difference in the electrical constant is created between the medicine and the human body.

We first examined various parameters that affect the outside electric field fluctuations associated with electromagnetic materials by using an electromagnetic field simulation. Then, we selected substances to be mixed with the medicine from 16 types of electromagnetic materials. Afterwards, we experimentally measured the outside electric field changes from the medicine. Lastly, we showed the effectiveness of this proposed method by obtaining the detection rate from the measurement results.

This paper is organized as follows. Section 2 describes the basic principle of electromagnetic material detection. Section 3 describes the electromagnetic field simulation for various parameters. Section 4 describes the experimental measurement of scattered field fluctuations caused by electromagnetic materials. Section 5 describes the characteristic evaluation of the detection rates of electromagnetic materials. Section 6 presents the conclusions of this study.

2. The Basic Principle of Electromagnetic Material Detection

Next, we describe the mathematical model of the scattered electric field used in this study. In the EM imaging method used in this research, we observe the effect of medication on scattered electromagnetic fields. First, we assumed an infinite length cylinder as the human model, and considered a case where the plane wave has only a component perpendicular to the cross-section of a cylinder. The scattered electric fields generated by the two-dimensional human model are expressed by a nonlinear integration equation [10–13], shown below.

$$E^s(x,y) = -(jk^2/4)\iint_s \tilde{\varepsilon}_r(x',y')\mu(x',y')E^{total}(x',y') H_0^{(2)}(k\rho)dx'dy' \quad (1)$$

where (x,y) and $(x^{'},y^{'})$ are observation points outside the human body and source points inside the body, respectively. $H_0^{(2)}$ is a zero-order second-kind Hankel function, k is the wave number, and ρ is the distance between an observation point and a source point. The total electric fields E^{total} in the human body can be expressed by the sum of the incident electric fields E^i and the scattered fields E^s, and are expressed by the following equation.

$$E^{total} = E^i + E^s \quad (2)$$

Previous studies have shown that the scattered electric field measured outside the human body changes depending on the presence or absence of a dielectric material that does not have a specific permeability of 1 and is not the same as air inside the body [14]. Therefore, it can be seen using Equation (2) whether the scattered electric field E^s changes depending on the electromagnetic material, and also when the total electric field E^{total} changes. In this study, we continuously measured the changes in the total electric field before and after swallowing and after the removal of the medicine. Lastly, the medicine detection was achieved by measuring the changes in the total electric field due to the movement of the medicine.

3. Examination of Various Parameters Using Electromagnetic Field Simulation

We conducted a three-dimensional electromagnetic field simulation by using the finite-difference time-domain (FDTD) method. The FDTD simulation was performed using

SEMCAD X ver.20.0 (Schmid and Partner Engineering AG), which is an electromagnetic simulator based on the FDTD method [15,16]. For the boundary condition of the FDTD simulation, we employed a perfectly matched layer (PML). For the time resolution of the FDTD method, we applied the Courant stability condition, defined as [17]

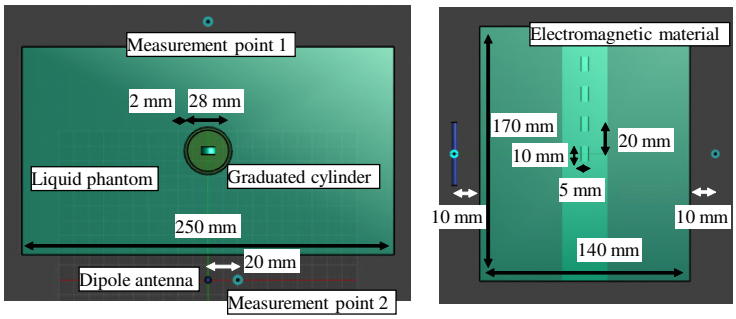
$$c\Delta t \leq \frac{1}{\sqrt{\frac{1}{\Delta x^2} + \frac{1}{\Delta y^2} + \frac{1}{\Delta z^2}}} \tag{3}$$

where c, Δt, Δx, Δy, and Δz are the speed of light, the time step, and the mesh size in the x, y, and z axes, respectively. Based on the above stability condition, we determined the time step Δt required to obtain stable results in the FDTD analysis. The voxel size (mesh size) was set to $\Delta x = \Delta y = \Delta z = 1$ mm, whose size satisfied the $1/10$ wavelength condition in the FDTD method at the employed frequencies. The trade-off relationship between computation time and degrees of freedom in the FDTD method has so far been discussed in [18,19]. It is to be noted that the FDTD method performs a full-wave simulation that can consider electromagnetic phenomena, including reflections, interference, etc. Also, the FDTD method is widely used in electromagnetic field analysis, such as for specific absorption rate (SAR) evaluation, so the reliability of the FDTD method can be confirmed from several related works [20,21]. An error analysis of the FDTD method was conducted in [22], where it was shown that the FDTD calculation can achieve an acceptable calculation error in a numerical model.

A model used in our electromagnetic field simulation is shown in Figure 1 and the parameters used are shown in Table 1. In the experiment of this study, a graduated cylinder is used to create an air layer for moving the electromagnetic material to a liquid phantom equivalent to a human body. For simplification purposes, we simplified the human model with a phantom model, whose reliability has been validated in [23].

Table 1. Simulation parameters.

Frequency of Incident Wave (GHz)		**2, 3, 4, 5**
Liquid phantom	Relative permittivity	37.93
	Conductivity (S/m)	0.536
Glass material	Relative permittivity	4.6
	Conductivity (S/m)	10^{-10}
Dielectromagnetic test materials	Relative permittivity	4
	Conductivity (S/m)	0, 10, 10,000
	Relative permeability	1, 100



(a) Top view (b) Side view

Figure 1. Simulation model.

In this simulation, to focus on the investigation of the effect on the detection accuracy of the permeability change in the test materials, we fixed the dielectric parameters of the liquid phantom. Therefore, the electromagnetic field simulation environment was simulated by creating a similar glass layer and an air layer. We defined the electromagnetic material at 0 mm when it was at the center of the liquid phantom, and then performed the electromagnetic field simulations as it was moved upwards to 60 mm. In addition, we selected 2 GHz to 5 GHz as the frequencies to be examined in the simulation in consideration for the miniaturization of an antenna and the influence of attenuation [23,24].

First, Figure 2 shows the change in the phase difference of the total electric field depending on the presence or absence of the electromagnetic material when the conductivity and relative permeability of the electromagnetic materials are changed.

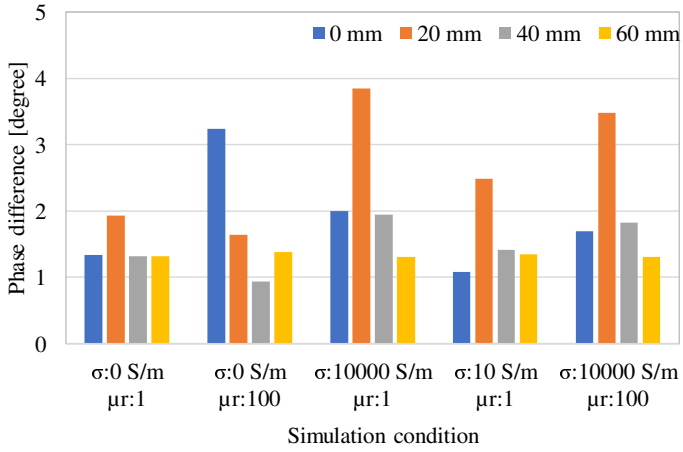


Figure 2. Changes in scattered electric field when the electrical and magnetic constants of electromagnetic materials are changed.

Comparing the graphs of the three patterns on the left side of Figure 2, it can be confirmed that the phase change is sensitive to not the magnetic permeability but the conductivity; in other words, the conductivity affects the phase change more strongly than the magnetic permeability. Furthermore, by comparing the graphs of the three patterns on the right side, it can be confirmed that increasing the conductivity of the electromagnetic material leads to a larger change in the total electric field. It can also be confirmed that when the conductivity of the electromagnetic material whose relative permeability is not 1 is set to 10,000 S/m, there is almost no effect on the total electric field due to the change in relative permeability. From the above results, we decided on using a conductivity of 10,000 S/m and a relative permeability of 1 for the electrical constants of the electromagnetic material. Next, Figures 3 and 4 show the changes in the phase difference (between before/after the electromagnetic material is inserted) when the measurement point is placed on the front and on the back of the liquid phantom, respectively. Comparing Figures 3 and 4, it can be verified that the phase change when the measurement point is placed behind the human body is larger at all frequencies. Also, from Figure 4, it can be seen that the changes in the total electric field are larger at 3 GHz and 4 GHz. Next, Figure 5 shows the rate of change in the intensity of the total electric field with or without electromagnetic material. From Figure 5, the rate of change is 6% or more at the two positions when the medicine is placed at 3 GHz and 4 GHz. Therefore, it can be concluded that it is appropriate to use 3 GHz or 4 GHz when measuring the changes in the intensity of the total electric field.

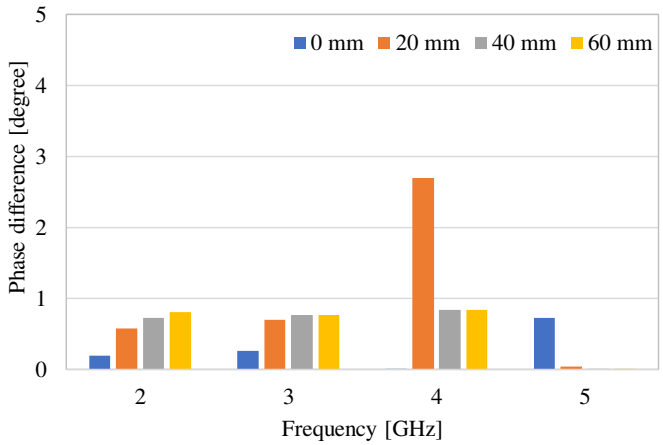


Figure 3. Simulation results of phase change when the measurement point is placed on the front of the human body.

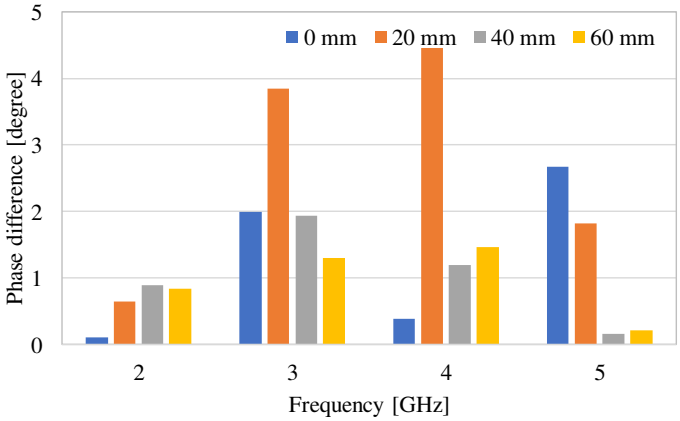


Figure 4. Simulation results of phase change when the measurement point is placed on the back of the human body.

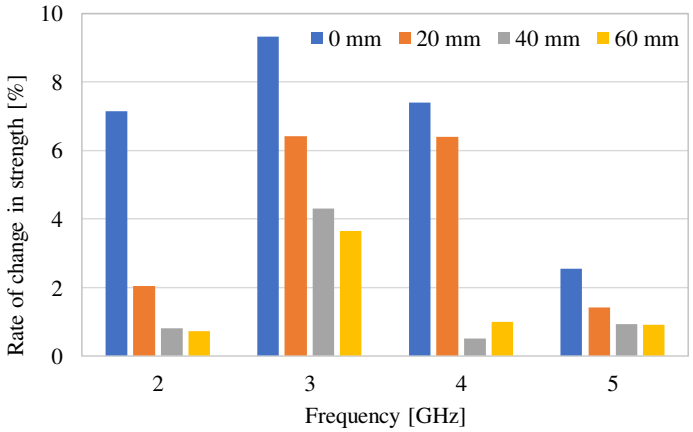


Figure 5. Simulation results of rate of change in the intensity of the total electric field with or without electromagnetic material.

4. Experimental Measurement of Scattered Field Fluctuations Caused by Electromagnetic Materials

4.1. Selection of Electromagnetic Materials

Notably, in Table 2 we determined the range of dielectric parameters, namely, relative permittivity, conductivity, and relative permeability, based on 16 kinds of test materials used in the experiment. We confirmed that all of the materials in Table 2 can be used in

medicines. Additionally, as for the human safety of electromagnetic waves, according to the ICNIRP guideline [25], a local peak specific absorption rate (SAR) as averaged over any ten grams should never exceed 2 W/kg for general exposure (or 10 W/kg for occupational exposure). Through preliminary simulation evaluation, we confirmed that the local SAR did not exceed 2 W/kg in the measurement setup. Figure 6 shows the experimental environment used for the selection. We used 2.1 GHz as the incident wave frequency. First, we put the medicine with a 1 cm diameter on the tip of a plastic jig and submerged it in the liquid phantom. Next, we selected the material by calculating the change in the total electric field before and after submerging the jig. Then, we measured the two patterns of electromagnetic material positions, as shown in Figure 7. Table 3 shows the measurement result of the changes in the received power with and without the electromagnetic material. Here, the amount of change in the received power depends on the amount of change in the scattered electric field. Therefore, we chose to use magnesium oxide, as it was one of the substances that changed significantly, as shown in Table 2. The difference between the simulation and measurement comes from the different settings, such as the existence of cables, different dielectric parameters of the test materials, and so on. However, from the results, a similar tendency was observed in the simulation and experiment, which indicates the possibility of detecting the electromagnetic materials using the EM imaging method.

Table 2. List of the electromagnetic materials chosen for the tests.

Sample Number	Test Material
1	Maghemite
2	Hematite
3	Magnetite
4	Black iron oxide treated with metaphosphate
5	Epsilon-type iron oxide
6	Anhydrous calcium hydrogen phosphate
7	Calcium carbonate
8	Titanium oxide
9	Magnesium oxide
10	Magnesium aluminate silicate
11	Magnesium silicate
12	Synthetic aluminum silicate
13	Dry aluminum hydroxide gel
14	Amber Light IRP88
15	Amber Light IRP69
16	Carbon microcoil (CMC)

4.2. Experimental Measurement of Changes in Total Electric Field

The experimental environment is shown in Figure 8. We conducted the experiment in a five-sided anechoic chamber. We amplified the incident power to 40 dB and used a dipole antenna and for the incident wave frequencies we used 3 GHz and 4 GHz.

Next, we will describe how we moved the electromagnetic materials in the experiment. First, we put the electromagnetic material, attached to a string, into a graduated cylinder inside the liquid phantom. After that, we used the string to move the electromagnetic material down and then up for a distance of 15 cm and for a total time of 20 s. When performing the measurement using LabVIEW, the electromagnetic material was moved for 50 s, and then a measurement without the electromagnetic material was performed for another 50 s. Then, we smoothed out the measured results by moving the average, as

the thermal noise caused by the amplifier was shown to be too large. These smoothed-out measurement results are shown in Figures 9 and 10. From Figures 9 and 10, it can be seen that the phases of both the 3 GHz and 4 GHz changes by about 2 degrees depending on the electromagnetic material. Furthermore, the phase changes due to the movement of the electromagnetic material can be confirmed at around 20 s at 3 GHz and at around 15 s at 4 GHz. In addition, it can be confirmed that the intensity changes by 2.6% and 5.6% at the maximum at 3 GHz and 4 GHz when converted to the electric field, respectively.

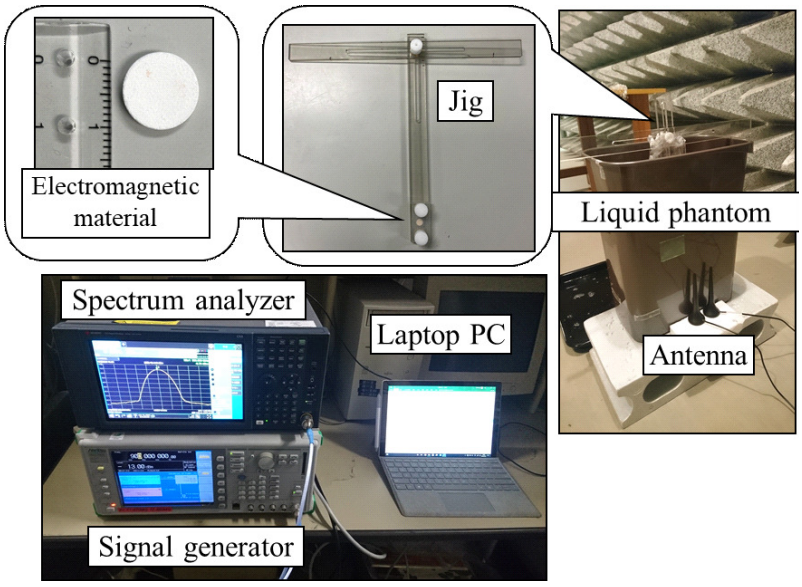


Figure 6. Experimental environment.

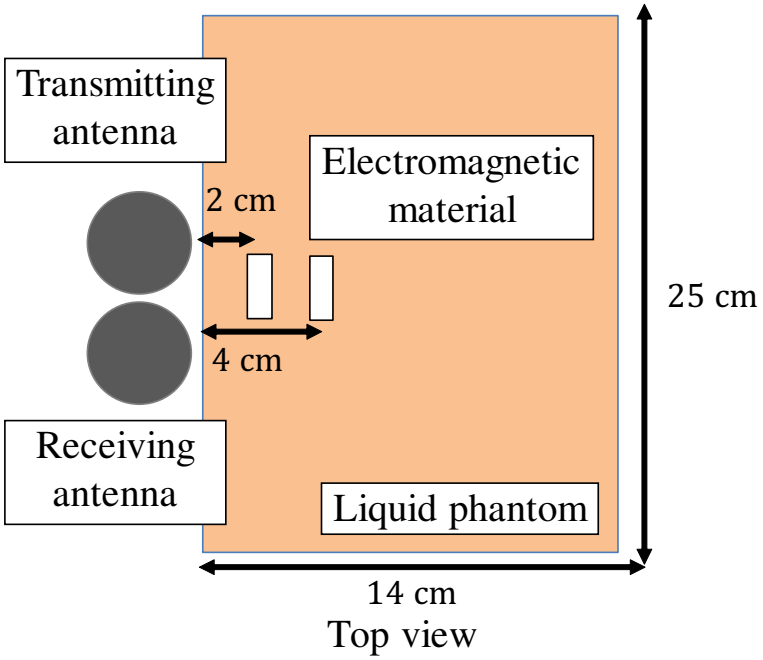
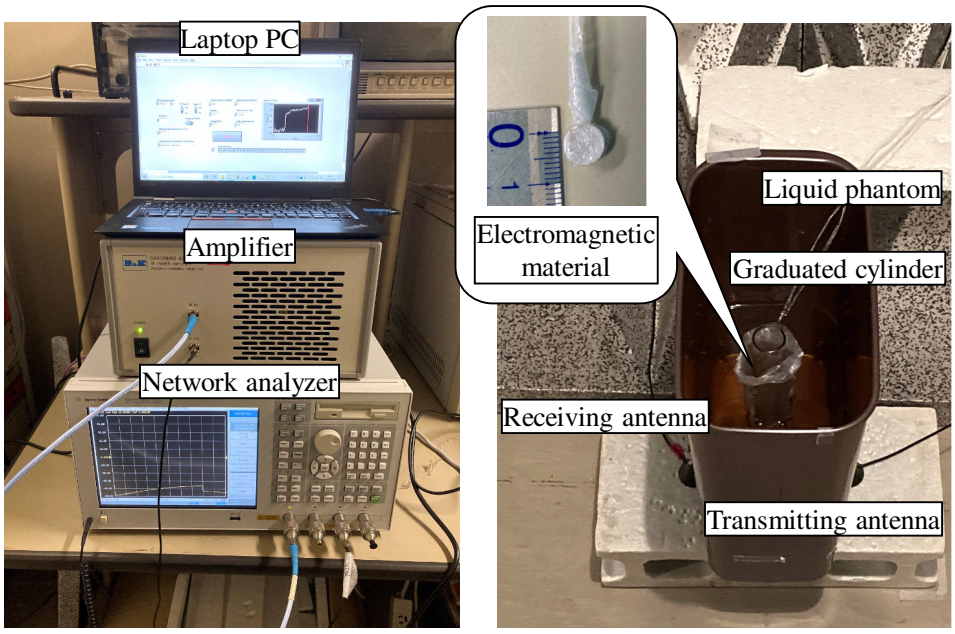


Figure 7. Placement position of the electromagnetic material.

Table 3. Changes in received power due to each substance used.

Sample Number	Received Power Change [dB]	
	2 cm	**4 cm**
1	36.8	0.7
2	8.6	0.2
3	19.4	0.7
4	24.5	2.3
5	4.9	0.9
6	33.7	1.4
7	12.5	2.6
8	23.3	2.6
9	29.1	3
10	25.6	2.3
11	7.6	3.3
12	4.5	1.2
13	11.3	2.8
14	15.6	0.2
15	39.3	0.2
16	12.9	1.6



(a) Outside the anechoic chamber (b) Inside the anechoic chamber

Figure 8. Experimental environment.

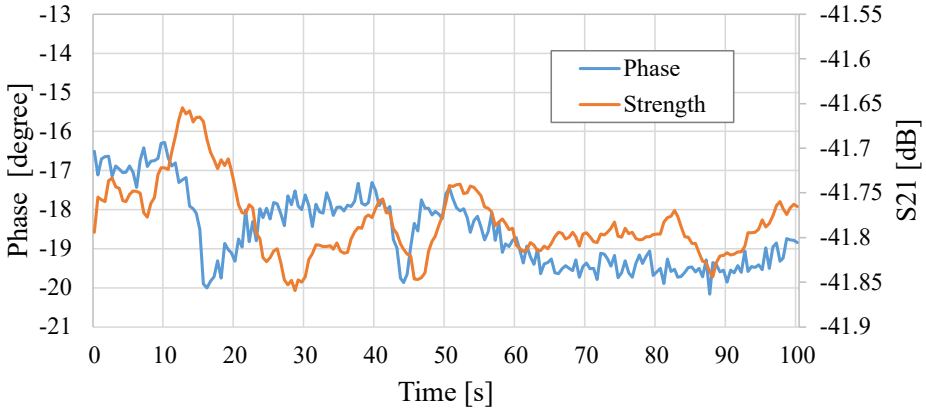


Figure 9. Measured results of the measured phase and strength of waveform at 3 GHz.

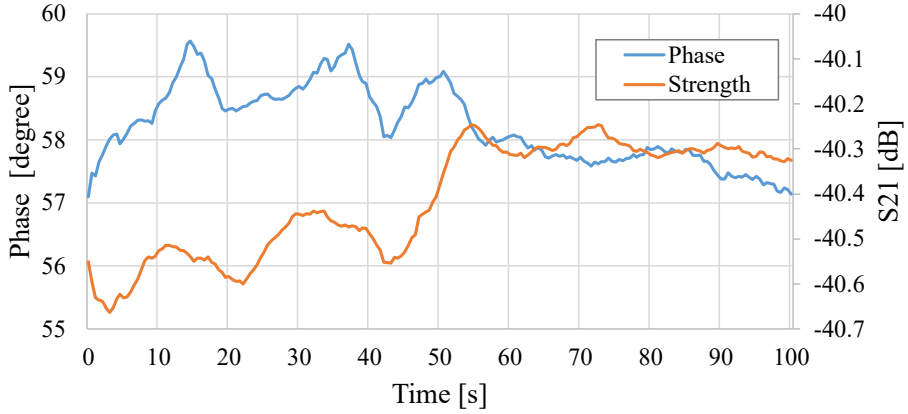


Figure 10. Measured results of the measured phase and strength of waveform at 4 GHz.

Finally, let us compare the results of the electromagnetic simulations and experimental measurements. Table 4 summarizes the comparison results between the simulation and measurements. In order to calculate the phase change in the measurement, we evaluated the difference in the average phases before (0 s–50 s) and after (50 s–100 s) the medication was removed. We can observe similar characteristics, with an acceptably small difference of below 0.52 degrees. Therefore, the applicability of our proposed method for medication detection is confirmed through electromagnetic simulation and measurement.

Table 4. Comparison between simulation and measurement results.

			Frequency	
			3 GHz	4 GHz
Phase difference (degree)	Simulation	0 mm	0.27	0.01
		20 mm	0.70	2.70
		40 mm	0.76	0.84
		60 mm	0.76	0.84
	Measurement		1.28	0.88
Difference between measurement and simulation (60 mm) (degree)			0.52	0.04

5. Characteristic Evaluation of Detection Rate of Electromagnetic Materials

5.1. Proposal of Electromagnetic Material Detection Algorithm

In this study, we detected the time when the electromagnetic material is taken in by reversing the time axis of the measured waveform. First, we need to explain the conventional method based on maximum likelihood estimation, which is often used in binary discrimination problems. The probability density function before and after the electromagnetic material is taken in is expressed by the following equation:

$$p_0 = \frac{i}{\sqrt{2\pi}\sigma_i} e^{-\frac{(x-\mu_j)^2}{2\sigma_i^2}} \ (i = 0, 1) \tag{4}$$

where σ_0, σ_1 and μ_0, μ_1 are the standard deviation and average value of the measured waveform before or after taking in the electromagnetic material, respectively. Also, x is the measured value of the total electric field at the current time. When the calculated p_0 and p_1 are compared at each time, the time when p_1 becomes larger is estimated as the detection timing.

Next, the threshold detection method can be explained as follows. First, we calculate the average value μ in the absence of the medicine. Then, we determine the threshold as S. After that, the time of the measured value that satisfies the following equation is estimated as the detection timing.

$$|x - \mu| > S \tag{5}$$

Here, x is the measured value of the total electric field at the current time. In this study, we searched for the optimum threshold with the highest detection rate for all measurement results by changing the threshold S. As an example, Figure 11 shows the changes in the detection rate due to the threshold when detecting from the phase measurement at 4 GHz.

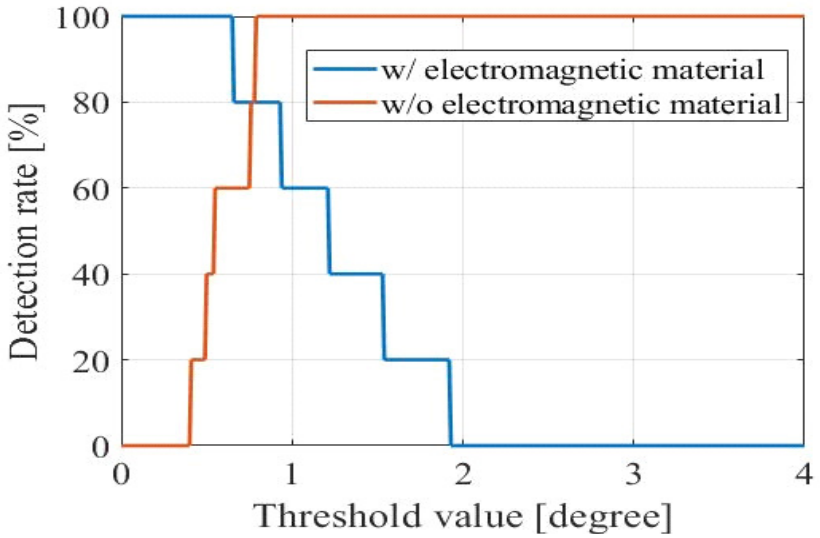


Figure 11. Change in the detection rate due to the threshold.

Then, the result without electromagnetic material is expressed as the detection rate by subtracting the false detection rate from 100%.

From Figure 11, it can be confirmed that the average value of the two detection rates is 90% at the optimum threshold of 0.9 (deg). Lastly, we present our proposed method, and in Figure 12 we can see the flowchart of the proposed algorithm. First, the waveform is smoothed out by obtaining the preceding moving average from the measured values. Then, the standard deviation at T', which is the cycle of moving the medicine from the start of measurement, is calculated as $\sigma_{T'}$ and is kept as the reference value in the absence of any

electromagnetic material. The standard deviation in the interval $x - T'$ to x is expressed as σ_x. The number of data N in the interval is given by

$$N = T'\Delta t \tag{6}$$

and $\sigma_{T'}$ is expressed by the following equation.

$$\sigma_{T'} = \sqrt{\frac{1}{N}\sum_{i=1}^{N}(x_i - \overline{x})^2} \tag{7}$$

Here, Δt is the sampling period. In addition, x_i is the measured value at each time and $\overline{x}$ is the average value of the interval. Then, the standard deviation when the interval is moved by the sampling period Δt is calculated and compared with twice the reference value if there is no detected electromagnetic material. As a result of this comparison, if the standard deviation of the current time is small the standard deviation of the sampling period Δt is moved and re-calculated, and the same procedure is repeated. On the other hand, if the standard deviation of the current time exceeds the reference value, the result can then be estimated as the detection timing. In this study, the time T was 100 s.

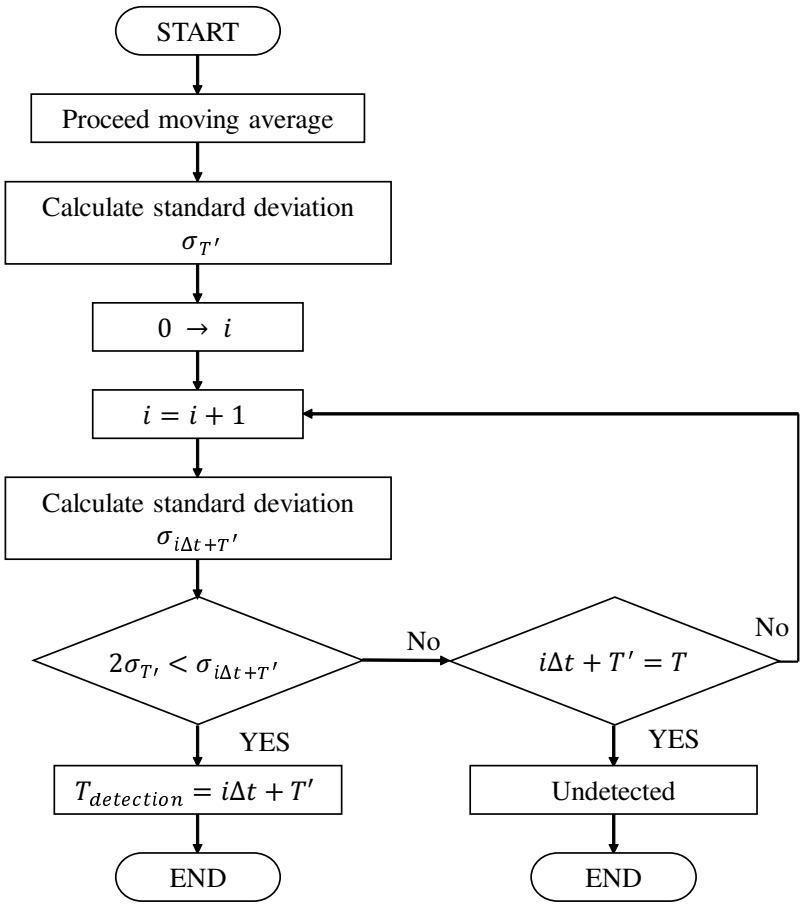


Figure 12. Flowchart of the proposed method.

5.2. Experimental Evaluation of Electromagnetic Material Detection Rate

We calculated the detection rate by measuring the changes in phase and intensity five times at 3 GHz and 4 GHz. The false positive rate was also calculated by conducting experiments without electromagnetic materials. Figures 13 and 14 show the average detection rate of the intensity and phase at each frequency. In this part, the miss detection rate is the probability that it will be determined not to be present when there is medicine,

and the false detection rate is the probability that it will be determined to be present when there is no medicine.

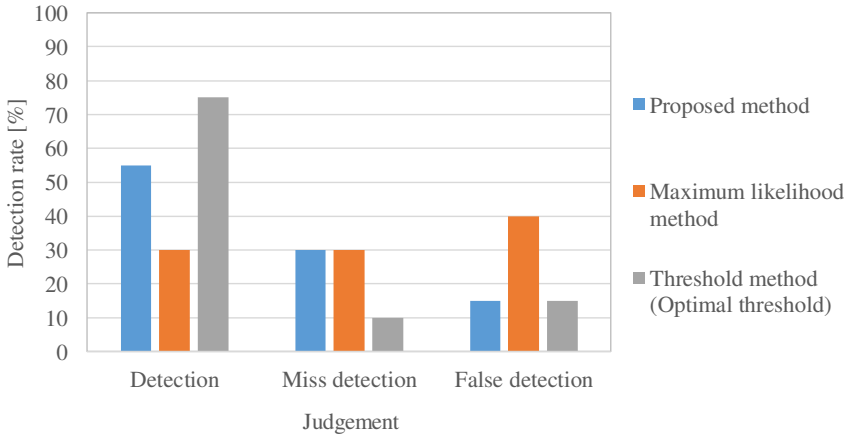


Figure 13. Comparison of detection rates using a conventional method and our proposed method (3 GHz).

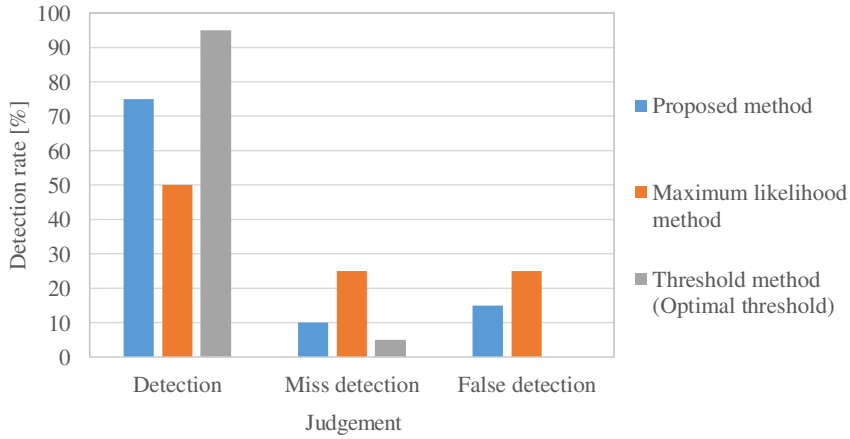


Figure 14. Comparison of detection rates using a conventional method and our proposed method (4 GHz).

Comparing the proposed method and the maximum likelihood method from Figures 13 and 14, it can be confirmed that the proposed method achieves better detection accuracy and it is also appropriate to use 4 GHz for the incident wave. Furthermore, when comparing the proposed method and the threshold method, it can be confirmed that the proposed method achieves a detection accuracy approaching the optimum threshold method obtained by post-processing. Also, comparing the false detection rates, it can be confirmed that the proposed method achieves lower rates than the maximum likelihood method due to the use of time-series data.

6. Conclusions

In this paper, we have aimed to detect medication based on the electric field outside the body that changes due to medicine with electromagnetic materials incorporated. Notably, compared with existing systems, our proposed system is a simple and non-intrusive method to track in-body materials (medication in this research), which can contribute to future healthcare advances, such as medication adherence. It should be noted that this paper demonstrates the possibility that EM imaging can be used for medication adherence, which strongly contributes to removing wireless communication circuits from pills for digital medicine applications. Simulations have shown that it is preferable to use either 3 GHz or 4 GHz as the incident wave and also to place the measurement point behind the

human body. We conducted experiments based on the simulation results, and obtained the detection rate of the electromagnetic material from the measurement results. The proposed method achieved better detection accuracy compared to the maximum likelihood method. Furthermore, when compared with the threshold method, it can be confirmed that the proposed method achieved a detection accuracy approaching the optimum threshold method obtained by post-processing.

As future work, we propose studying a method using realistic transmission power and to perform electromagnetic field simulations as well as experiments when considering movements of the body. One of our future subjects is to conduct in vivo experiments to evaluate our proposed system in a realistic situation considering the anisotropics of the test materials. Furthermore, an error analysis of the numerical calculation and the detection mechanism from the viewpoint of theoretical analysis are also important future subjects. As for other future works, we will consider the traceable time before pills are dissolved, although we have not discussed the time until pills dissolve in this paper. Also, another future subject is to discuss the sensitivity of the proposed method, because the change in the electric fields should be larger than the noise component for realizing reliable medication detection.

Author Contributions: Conceptualization, J.H. (Junya Hoshino) and D.A.; methodology, J.H. (Junya Hoshino); software, J.H. (Junya Hoshino); validation, J.H. (Junya Hoshino), T.K. and D.A.; formal analysis, J.H. (Junya Hoshino); investigation, J.H. (Junya Hoshino); resources, D.A.; data curation, J.H. (Junya Hoshino); writing—original draft preparation, J.H. (Junya Hoshino); writing—review and editing, J.H. (Jaakko Hyry); visualization, T.K. and J.H. (Junya Hoshino); supervision, D.A.; project administration, D.A.; funding acquisition, D.A. All authors have read and agreed to the published version of the manuscript.

Funding: This research and developement was supported in part by JST Moonshot R&D Grant Number JPMJMS2214-06 and MIC/SCOPE #JP225006004.

Data Availability Statement: The raw data supporting the conclusions of this article will be made available by the authors on request.

Conflicts of Interest: The authors declare no conflict of interest.

Abbreviations

The following abbreviations are used in this manuscript:

BAN	Body area network
WCE	Wireless capsule endoscopy
EM	Electromagnetic
RSSI	Received signal strength indicator
TOA	Time of arrival
CT	Computed tomography
FDTD	Finite-difference time-domain
MRI	Magnetic resonance imaging
SAR	Specific absorption rate

References

1. Wang, J.; Wang, Q. *Body Area Communications: Channel Modeling, Communication Systems, and EMC*; John Wiley & Sons: Hoboken, NJ, USA, 2012. [CrossRef]
2. Otto, C.; Milenković, A.; Sanders, C.; Jovanov, E. System architecture of a wireless body area sensor network for ubiquitous health monitoring. *J. Mob. Multimed.* **2006**, *1*, 307–326. [CrossRef]
3. *802.15.6-2012*; IEEE Standard for Local and metropolitan area networks—Part 15.6: Wireless Body Area Networks. IEEE: Piscataway, NJ, USA, 2012. [CrossRef]
4. Hafezi, H.; Robertson, T.L.; Moon, G.D.; Au-Yeung, K.Y.; Zdeblick, M.J.; Savage, G.M. An ingestible sensor for measuring medication adherence. *IEEE Trans. Biomed. Eng.* **2014**, *62*, 99–109. [CrossRef] [PubMed]

5. Otsuka Pharmaceutical Co., Ltd. Otsuka and Proteus Announce the First U.S. FDA Approval of a Digital Medicine System: ABILIFY MYCITE (Aripiprazole Tablets with Sensor). Available online: https://www.otsuka.co.jp/en/company/newsreleases/2017/20171114_1.html (accessed on 8 January 2024).
6. Kawasaki, M.; Kohno, R. Position estimation method of medical implanted devices using estimation of propagation velocity inside human body. *IEICE Trans. Commun.* **2009**, *92*, 403–409. [CrossRef]
7. Pourhomayoun, M.; Fowler, M.; Jin, Z. A novel method for medical implant in-body localization. In Proceedings of the 2012 Annual International Conference of the IEEE Engineering in Medicine and Biology Society, San Diego, CA, USA, 28 August–1 September 2012; pp. 5757–5760. [CrossRef]
8. Xu, Y.; Dandan, W.; Hua, F. Underwater acoustic source localization method based on TDOA with particle filtering. In Proceedings of the 26th Chinese Control and Decision Conference (2014 CCDC), Changsha, China, 31 May–2 June 2014; pp. 4634–4637. [CrossRef]
9. Goh, S.T.; Zekavat, S.A.; Pahlavan, K. DOA-based endoscopy capsule localization and orientation estimation via unscented Kalman filter. *IEEE Sen. J.* **2014**, *14*, 3819–3829. [CrossRef]
10. Umashankar, K.; Taflove, A.; Rao, S. Electromagnetic scattering by arbitrary shaped three-dimensional homogeneous lossy dielectric objects. *IEEE Trans. Antennas Propag.* **1986**, *34*, 758–766. [CrossRef]
11. Wang, J. A Study on Noninvative Measurement of Dielectric Properties and Electromagnetic Wave Absorption of Biological Tissue. Ph.D. Thesis, Tohoku University, Sendai, Japan, 1991.
12. Richmond, J. Scattering by a dielectric cylinder of arbitrary cross section shape. *IEEE Trans. Antennas Propag.* **1965**, *13*, 334–341. [CrossRef]
13. Chew, W.C.; Wang, Y.M. Reconstruction of two-dimensional permittivity distribution using the distorted Born iterative method. *IEEE Trans. Med. Imaging* **1990**, *9*, 218–225. [CrossRef] [PubMed]
14. Kobayashi, H.; Anzai, D.; Wang, J. Em imaging-based capsule endoscope localization with peak-formed incident electric fields. In Proceedings of the 13th EAI International Conference on Body Area Networks, Oulu, Finland, 2–3 October 2018; Springer: Berlin/Heidelberg, Germany, 2020. [CrossRef]
15. Schmid & Partner Engineering AG. SEMCAD & Matterhorn. Available online: https://speag.swiss/products/semcad/overview/ (accessed on 8 January 2024).
16. Chavannes, N.; Fortunato, C.; Ofli, E.; Kuster, N. SEMCAD X matterhorn: A novel approach to achieve realism in highly complex environments. In Proceedings of the 2015 9th European Conference on Antennas and Propagation (EuCAP), Lisbon, Portugal, 13–17 April 2015; IEEE: Piscataway, NJ, USA, 2015; pp. 1–2.
17. Taflove, A.; Hagness, S.; Piket-May, M. *Computational Electrodynamics: The Finite-Difference Time-Domain Method*; Artech House: Norwood, MA, USA, 2005. [CrossRef]
18. Teixeira, F.L.; Sarris, C.; Zhang, Y.; Na, D.Y.; Berenger, J.P.; Su, Y.; Okoniewski, M.; Chew, W.C.; Backman, V.; Simpson, J.J. Finite-difference time-domain methods. *Nat. Rev. Methods Prim.* **2023**, *3*, 75. [CrossRef]
19. Sugimoto, S.I.; Takei, A.; Ogino, M. Finite element analysis with tens of billions of degrees of freedom in a high-frequency electromagnetic field. *Mech. Eng. Lett.* **2017**, *3*, 16-00667. [CrossRef]
20. Yu, W. *Electromagnetic Simulation Techniques Based on the FDTD Method*; John Wiley & Sons: Hoboken, NJ, USA, 2009; Volume 221.
21. Gaffar, M.; Jiao, D. An explicit and unconditionally stable FDTD method for electromagnetic analysis. *IEEE Trans. Microw. Theory Tech.* **2014**, *62*, 2538–2550. [CrossRef]
22. Cheng, Y.; Chen, G.; Wang, X.H.; Yang, S. Investigation of numerical dispersion with time step of the FDTD methods: Avoiding erroneous conclusions. *IET Microwaves, Antennas Propag.* **2021**, *15*, 691–703. [CrossRef]
23. Onishi, T.; Uebayashi, S. Biological tissue-equivalent phantoms usable in broadband frequency range. *NTT DoCoMo Tech. J.* **2006**, *7*, 61–65.
24. Kletsov, A.; Chernokalov, A.; Khripkov, A.; Cho, J.; Druchinin, S. Microwave non-contact imaging of subcutaneous human body tissues. *Healthc. Technol. Lett.* **2015**, *2*, 108–111. [CrossRef] [PubMed]
25. International Commission on Non-Ionizing Radiation Protection (ICNIRP). Guidelines for limiting exposure to electromagnetic fields (100 kHz to 300 GHz). *Health Phys.* **2020**, *118*, 483–524. [CrossRef] [PubMed]

Disclaimer/Publisher's Note: The statements, opinions and data contained in all publications are solely those of the individual author(s) and contributor(s) and not of MDPI and/or the editor(s). MDPI and/or the editor(s) disclaim responsibility for any injury to people or property resulting from any ideas, methods, instructions or products referred to in the content.